

AD-A126 351

SLIDING FORCES AND NORMAL LOADS ON PROJECTILE ROTATING
BANDS(U) MISSISSIPPI STATE UNIV MISSISSIPPI STATE DEPT
OF MECHANICAL ENGINEERING A K STIFFLER JAN 83

1/1

UNCLASSIFIED

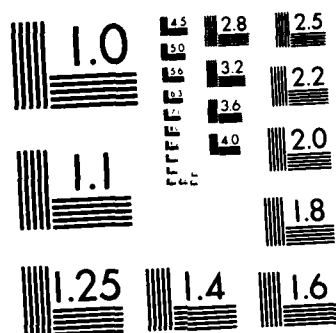
AFOSR-TR-83-0036 AFOSR-82-0169

F/G 19/1

NL

END

FILED
JAN 83
AFOSR



MICROCOPY RESOLUTION TEST CHART
NATIONAL BUREAU OF STANDARDS-1963 A

2036

(11)

AD A 126351

Sliding Forces and Normal Loads On Projectile Rotating Bands

A. Kent Stiffler

Mississippi State University
Department of Mechanical Engineering
Mississippi State, MS 39762

January 1983

FINAL REPORT for Minigrant
AFOSR-82-0169

Sponsored by

The Air Force Office of Scientific Research
Bolling AFB, Washington DC 20332

Approved for public release;
Distribution unlimited.

DTIC
NOTE
APR 5 1983

A

DTIC FILE COPY

83 04 05 165

Unclassified

SECURITY CLASSIFICATION OF THIS PAGE (When Data Entered)

| REPORT DOCUMENTATION PAGE | | READ INSTRUCTIONS BEFORE COMPLETING FORM |
|---|-----------------------|--|
| 1. REPORT NUMBER | 2. GOVT ACCESSION NO. | 3. RECIPIENT'S CATALOG NUMBER |
| | AD-A126 351 | |
| 4. TITLE (and Subtitle) Sliding Forces and Normal Loads on Projectile Rotating Bands | | 5. TYPE OF REPORT & PERIOD COVERED Final Report 4/15/82 to 12/14/83 |
| | | 6. PERFORMING ORG. REPORT NUMBER |
| 7. AUTHOR(s) A. Kent Stiffler | | 8. CONTRACT OR GRANT NUMBER(s) AFOSR-82-0169 |
| 9. PERFORMING ORGANIZATION NAME AND ADDRESS Department of Mechanical Engineering Mississippi State University Miss. State, MS 39762 | | 10. PROGRAM ELEMENT, PROJECT, TASK AREA & WORK UNIT NUMBERS 61102 F 2307109 |
| 11. CONTROLLING OFFICE NAME AND ADDRESS AFOSR/NA Bolling AFB, DC 20332 | | 12. REPORT DATE January 1983 |
| | | 13. NUMBER OF PAGES 39 |
| 14. MONITORING AGENCY NAME & ADDRESS (if different from Controlling Office) | | 15. SECURITY CLASS. (of this report) Unclassified |
| | | 15a. DECLASSIFICATION/DOWNGRADING SCHEDULE |
| 16. DISTRIBUTION STATEMENT (of this Report) Approved for public release; distribution unlimited. | | |
| 17. DISTRIBUTION STATEMENT (of the abstract entered in Block 20, if different from Report) | | |
| 18. SUPPLEMENTARY NOTES The views and conclusions contained in this document are those of the author and should not be interpreted as necessarily representing the official policies or endorsements, either expressed or implied, of the Air Force Office of Scientific Research or the U.S. Government. | | |
| 19. KEY WORDS (Continue on reverse side if necessary and identify by block number) engraving projectile sliding forces friction | | |
| 20. ABSTRACT (Continue on reverse side if necessary and identify by block number) A theory is presented to determine the projectile sliding forces in interior ballistics. Emphasis is placed on the barrel entrance region where the projectile rotating bands are impelled on to the rifling. It is proposed that the contact stress is constant and is given by a modified von Mises failure criterion. Normal loads and friction forces are dependent on the growth of the contact area which is derived from the geometrical details of the projectile and barrel. Radial displacements at the contact are included. The theory is in agreement with quasi-static and dynamic laboratory tests. | | |

DD FORM 1 JAN 73 1473

EDITION OF 1 NOV 65 IS OBSOLETE
S/N 0102-LF-014-6601

SECURITY CLASSIFICATION OF THIS PAGE (When Data Entered)

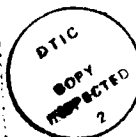
PREFACE

During the summer of 1981 the author worked at the Air Force Armament Laboratory, Interior Ballistic Branch, Eglin AFB under the AFOSR Summer Faculty Research Program (Contract F49620-79-C-0038). At that time he developed a theory for the normal loads and sliding forces encountered by projectiles when their rotating bands are engraved. The theory was extended to include those forces down bore as well.

The present minigrant (AFOSR-82-0169) is intended to modify the above theory to account for projectile and barrel radial displacements. These displacements are important for predicting the engraving forces found in the field where standard HEI hollow base projectiles, having flexible walls, and propellant gas pressures cause radial strain. Additional effort was spent on polymer dynamic flow pressure concepts.

The enclosed report represents the first comprehensive theory to predict projectile sliding forces in a rifled barrel. A copy has been sent to the International Journal of Mechanical Sciences for publication.

| | |
|-------------------|--|
| Accession For | |
| NTIS GRAM1 | <input checked="checked" type="checkbox"/> |
| DTIC TAB | <input type="checkbox"/> |
| Unannounced | <input type="checkbox"/> |
| Justification | |
| By _____ | |
| Distribution/ | |
| Availability Code | |
| _____ | |
| Print | Serial |
| A | |



SUMMARY

A theory is presented to determine the projectile sliding forces in interior ballistics. Emphasis is placed on the barrel entrance region where the projectile rotating bands are impelled on to the rifling. It is proposed that the contact stress is constant and is given by a modified von Mises failure criterion. Normal loads and friction forces are dependent on the growth of the contact area which is derived from the geometrical details of the projectile and barrel. Radial displacements at the contact are included. The theory is in agreement with quasi-static and dynamic laboratory tests.

NOTATION

| | |
|-----------------|---|
| A | band contact area |
| A_3 | maximum band contact area |
| A_p | projectile base area |
| A_p' | projectile cross-sectional area at the band |
| b_1, b_2 | exposed and submerged band thickness (Figure 4) |
| B | equation 49 |
| c_n | equation 50 |
| d_b | rotating band diameter |
| d_o | bore or rifling land diameter |
| d_1 | rifling groove diameter |
| d_2 | gun barrel diameter |
| E_b, E_p, E_o | modulus of elasticity for band, projectile, and barrel respectively |
| F_n | friction force, $\mu_n W_n$ |
| F_s | friction force, $\mu_s W_s$ |
| F_x | projectile sliding resistance force in x direction |
| F_y | projectile spin force in y direction |
| h | projectile wall thickness under the band |
| I | projectile rotational inertia |
| k | von Mises constant |
| ℓ | band length at bevel base |
| ℓ_1 | band length at bevel top |
| L | equation 1 |

| | |
|----------------------|--|
| m^-, m^+ | equations 14 and 17 respectively |
| M | total projectile mass |
| M' | projectile mass between the band and nose |
| P | gas pressure at projectile base |
| P' | projectile compressive stress at the band cross-section |
| P_i | gas pressure to un-crimp projectile from case |
| P_1 | gas pressure at start of engraving |
| P_2 | gas pressure at end of engraving |
| s | band contact length, $A/\pi d_b$ |
| W_n | load normal to band surface |
| W_s | load on the band from the rifling constraint which rotates projectile |
| x | projectile displacement along the barrel starting at band-cone contact |
| x_1, x_2, x_3 | projectile displacement to the end of regimes I, II, III respectively |
| X | projectile displacement along the barrel starting at crimped position |
| X_i | distance between x and X |
| y | projectile surface displacement in direction of rotation |
| α | angular displacement of projectile rotation |
| α_2, α_3 | band forward and rear bevel angle respectively (Figure 4) |
| γ | constant, equation 30 |
| δ_a | radial displacement of projectile due to acceleration |
| δ_b | radial displacement of band due to contact stress |
| δ_g | radial displacement of barrel due to gas pressure |
| δ_p | radial displacement of projectile due to contact stress |

| | |
|-----------------------|---|
| δ_o | radial displacement of barrel due to contact stress |
| δ_s | radial displacement of projectile due to spin |
| μ_n, μ_s | coefficient of friction; quasi-static conditions |
| μ_n', μ_s' | coefficient of friction; dynamic conditions |
| ν_b, ν_p, ν_o | Poisson's ratio for the band, projectile and barrel respectively |
| ϕ | forcing cone angle (Figure 3) |
| σ | compressive stress between band and barrel |
| σ_b | compressive stress at the band base |
| σ_f | band static flow pressure |
| σ_f' | band dynamic flow pressure |
| σ_s | band static yield pressure |
| σ_s' | band dynamic yield pressure |
| $\bar{\sigma}$ | equation 25 |
| τ | band shear stress |
| τ_s | band shear strength |
| θ | rifling angle of twist |
| ζ | constant, equation 25 |

Overscript

- derivative with respect to time

1.0 INTRODUCTION

The basic interior ballistic problem is to determine the energy release and corresponding pressure generated by the burning propellant in a variable volume, ultimately to establish the muzzle velocity of the projectile. The dynamics must account for certain losses which include rotating band frictional effects and heat transfer from the hot gases to the gun. Krier and Adams [1] report that frictional losses account for approximately two percent of the energy released by the propellants in medium caliber guns. Although direct friction losses appear small, they are important where an accurate prediction of projectile velocity is desired. In addition, friction can indirectly influence the thermodynamics and heat transfer processes which play a much larger role in predicting the projectile velocity. Small changes in the initial sliding forces can increase the peak gas pressures and temperatures by twenty percent [2].

Another problem in internal ballistics is gun life. Both erosion and wear can lead to barrel replacement after a few thousand rounds [3]. In the past rotating bands have been made from bronze (90 CU, 10 ZN), called gilding metal; however, recent success [4] with nylon bands suggest that they will be used extensively in the future. Plastic bands not only reduce sliding forces but improve gun life. The need for better velocity predictive codes and for an understanding of barrel wear has intensified interest in rotating band contact loads and sliding forces.

Spin is imparted to the projectile by a series of spiral grooves cut into the barrel to form the rifling, Figure 1. The elevated flat surface of the rifling, giving the bore diameter, is referred to here as the land, as opposed to the groove. A raised band, the rotating band, girds the projectile near its base. A tapered reamer is used to mill the barrel entrance. This process produces a fixed angle, decreasing from the rotating band diameter to the bore diameter (approximately the projectile diameter); it is called the "forcing cone". The solid rotating band first contacts the barrel just before the rifling. As the projectile proceeds, band material is gradually removed, both from the groove and the land, to accommodate the forcing cone. The additional material removed from the linearly rising rifling will lock the projectile to the rifling through the band. Figure 2 shows a projectile after it has passed through the forcing cone. The process described above is called the "engraving" process. It is completed within several bore diameters.

Frictional behavior in internal ballistics is exceedingly complex due to the large loading forces, high sliding velocities, and the nature of the dynamically changing interface between the projectile and barrel. Engraving and bore sliding force models take essentially two forms: (i) the frictional losses are assumed to be proportional to the kinetic velocity of the projectile [5]; (ii) a table of experimental sliding force as a function of projectile position is used or, more simply, a constant engraving force followed by a smaller constant bore force [6]. Estimates of these two forces are given as 10% and 1% of the maximum gas pressure. Recently, Fisher and Trippe [7] have divided the friction force into a linearly

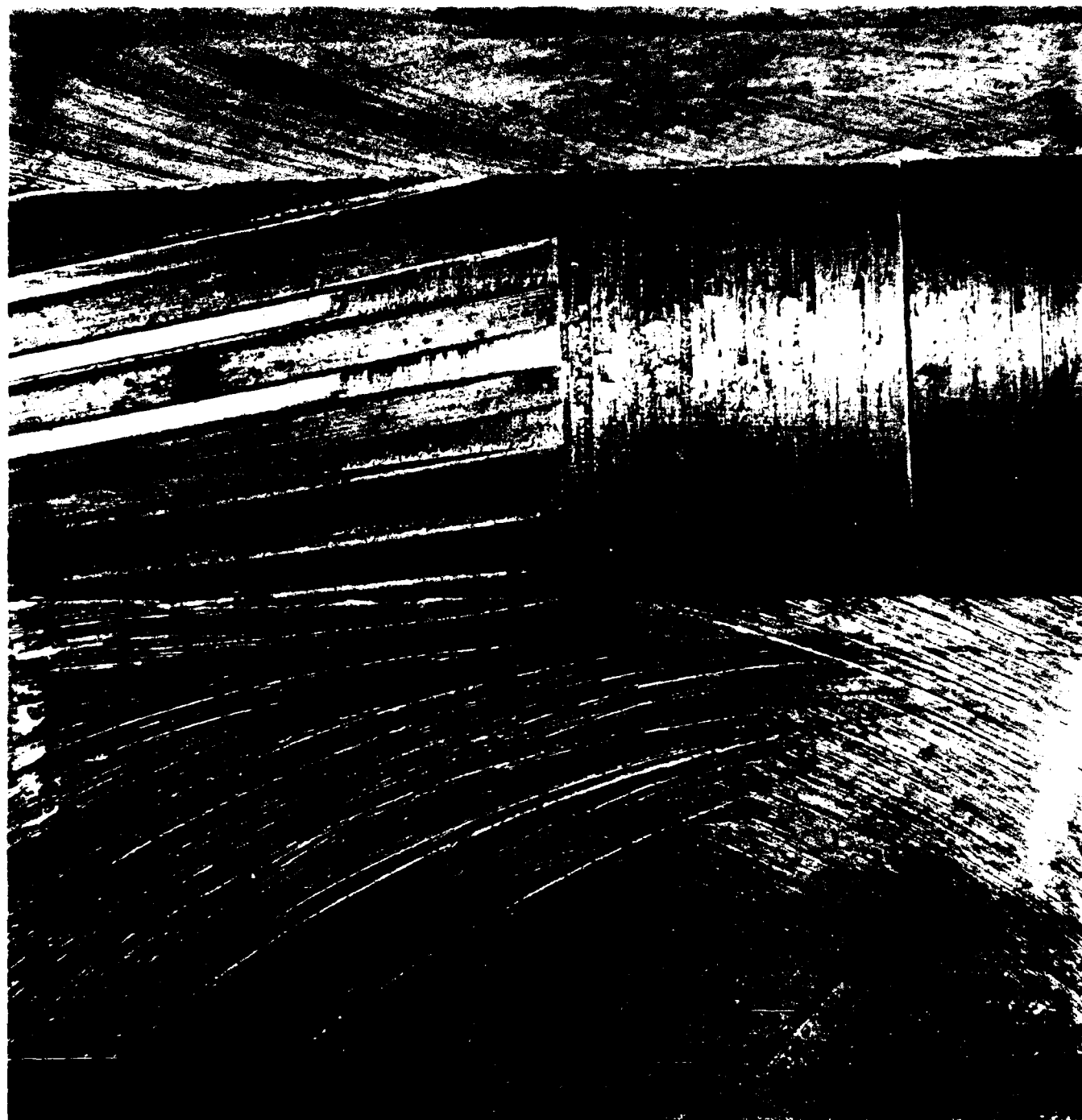


Fig. 1. Barrel Entrance with Riffing Start

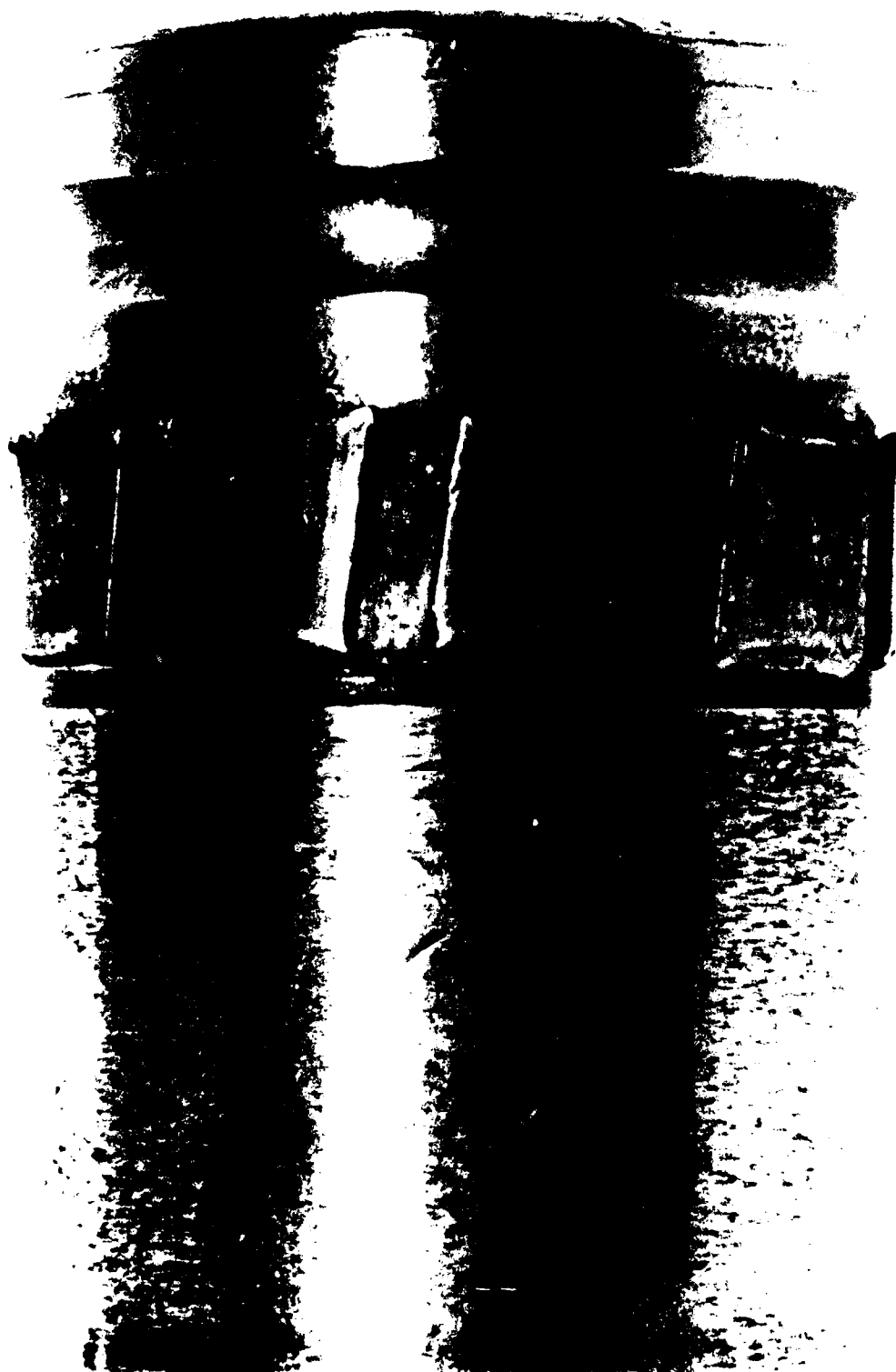


Fig. 2. Engraved Projectile Rotating Band

increasing force during the engraving process followed by a linearly decreasing force during the bore sliding process. This model is based upon data obtained from extruding brass and aluminum stock. In all cases empirical sliding forces are based on ad hoc conditions. This paper will develop a theory to explain projectile sliding forces.

2.0 PROJECTILE DYNAMICS

The geometrical relationship between the projectile and barrel in interior ballistics is shown in Figure 3. The rifling twists at some fixed angle θ although in some cases the angle may vary along the bore to reduce spin forces on the band during the peak acceleration. The forcing cone has a fixed angle ϕ to the bore. When the projectile is fired, the burning gases develop a pressure P_i at the projectile base to overcome a crimping force before the projectile is displaced a distance X from its breach position. It will proceed a short distance X_i before the rotating band makes contact with the forcing cone, designated by coordinate system x . At this point the band is engraved onto the rifling as the projectile travels a distance

$$L = (d_b - d_o)/2 \tan\phi \quad (1)$$

where d_b is the band diameter and d_o is the bore or rifling land diameter. As the band is being engraved, it is subjected to a load W_n normal to the rifling land, producing a sliding force F_n along the land surface. In addition the rifling twist causes a spin load W_s normal to the rifling face, producing a second sliding force along the face.

For the post-engraving region the following equations can be written for the axial and rotational acceleration of the projectile:

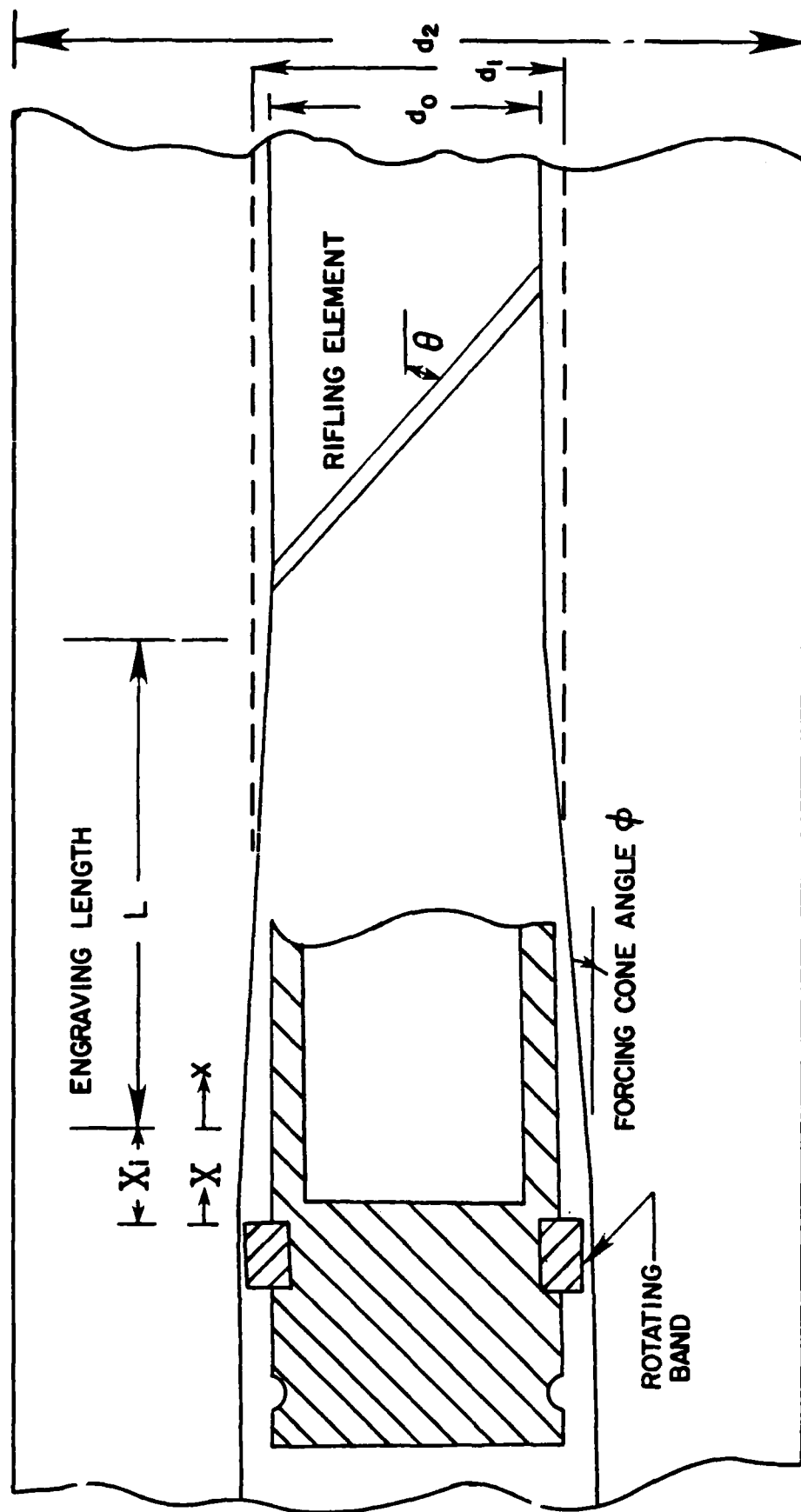


Fig. 3 Engraving geometry

$$M\ddot{x} = PA_p - F'_x \quad (2)$$

$$I\ddot{\alpha} = d_b F_y / 2 \quad (3)$$

where M , I , A_p are the projectile mass, rotational inertia, and base area respectively, and

$$F'_x = W_s \sin\theta + (F_n + F_s)\cos\theta \quad (4)$$

$$F_y = W_s \cos\theta - (F_n + F_s)\sin\theta \quad (5)$$

Now the rotational surface velocity \dot{y} of the projectile is related to the axial velocity \dot{x} through the rifling constraint:

$$\dot{y} = \dot{x} \tan\theta$$

or

$$\ddot{y} = \ddot{x} \tan\theta + \dot{x}^2 d(\tan\theta)/dx \quad (6)$$

with $\ddot{y} = d_b \ddot{\alpha} / 2$. Writing the sliding forces in terms of the normal loads,

$$F_s = \mu_s W_s \quad (7)$$

$$F_n = \mu_n W_n \quad (8)$$

where μ is the coefficient of sliding friction, and eliminating W_s through equation (3), equation (2) becomes

$$M\ddot{x} + \frac{4I(\mu_s + \tan\theta)}{d_b^2(1 - \mu_s \tan\theta)} [\ddot{x} \tan\theta + \dot{x}^2 \frac{d(\tan\theta)}{dx}] = PA_p - F_x \quad (9)$$

where

$$F_x = \frac{W_n \mu_n}{\cos\theta - \mu_s \sin\theta} \quad (\text{post-engraving}) \quad (10)$$

During the engraving process, the axial force F_n must be adjusted for the forcing cone angle ϕ . Furthermore, the normal load W_n on the land surface now has a component opposing the axial motion. Thus,

$$F_x = \frac{W_n \mu_n \cos\phi}{\cos\theta - \mu_s \sin\theta} + W_n \sin\phi$$

Generally, the rifling is cut without a twist for the engraving process to reduce shear forces which could strip the bands during this critical period. Thus, the engraving resistance force for small rifling twist is simply

$$F_x = W_n (\mu_n \cos\phi + \sin\phi) \quad (\text{engraving}) \quad (11)$$

3.0 QUASI-STATIC ENGRAVING THEORY

Most of the engraving force data in the literature show considerable variation among force-displacement curves because there is little uniformity in the rotating band, forcing cone, and barrel groove dimensions [8][9]. Bronze bands have compounded the problem because material of the same composition can vary by a factor of two depending on the degree of work hardening. It is imperative then to focus on the projectile-barrel geometry and band properties.

Let the engraving process begin with point contact between the band and forcing cone. Before the projectile moves, the material at this point must yield or flow. As movement commences, additional material begins to flow as it is pushed to the rear of the band. A simple calculation will show that only a small fraction of the material is actually taken up in strain. The following model of the engraving process is proposed.

(1) It is assumed that the stress between the band and cone surface remains constant and is given by the material flow pressure σ_f under quasi-static conditions. Then

$$F_x = \sigma_f A (\mu_n \cos\phi + \sin\phi) \quad (12)$$

where A is the contact area.

(2) It is assumed that the engraving force increase with displacement is caused by growth of the contact area.

Based upon these assumptions, several regimes develop in the force-displacement curves.

3.1 Regime I

In the case to be considered, the band diameter exceeds the rifling groove diameter and contact will occur over the circumference including land and groove. The force and area will increase linearly as the band moves into the fixed cone angle. If the band diameter is less than the rifling groove diameter, initial contact will occur on the rifling surface. Later, contact also will take place on the groove, enhanced by the tendency of flowing band material from the land to enter the groove. Thus, the displacement curve will be broken by an initial shallower slope [9].

The contact geometry of the rotating band and rifling cone during engraving is given in Figure 4. The band may or may not have bevels cut to the projectile surface, but it is believed that beveling, which reduces the material to be removed and which gives more space for debris, improves the engraving process. A typical projectile displacement x will expose a band contact length $s_1 + s_2$. Then

$$A = d_b(s_1 + s_2)\pi \quad (13)$$

where

$$s_1 = x/\cos\phi \quad 0 \leq x \leq x_1$$

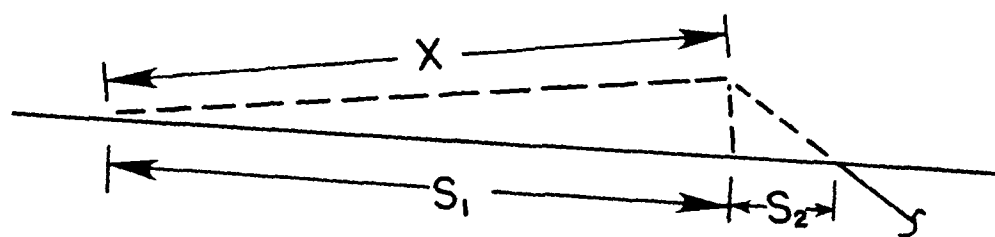
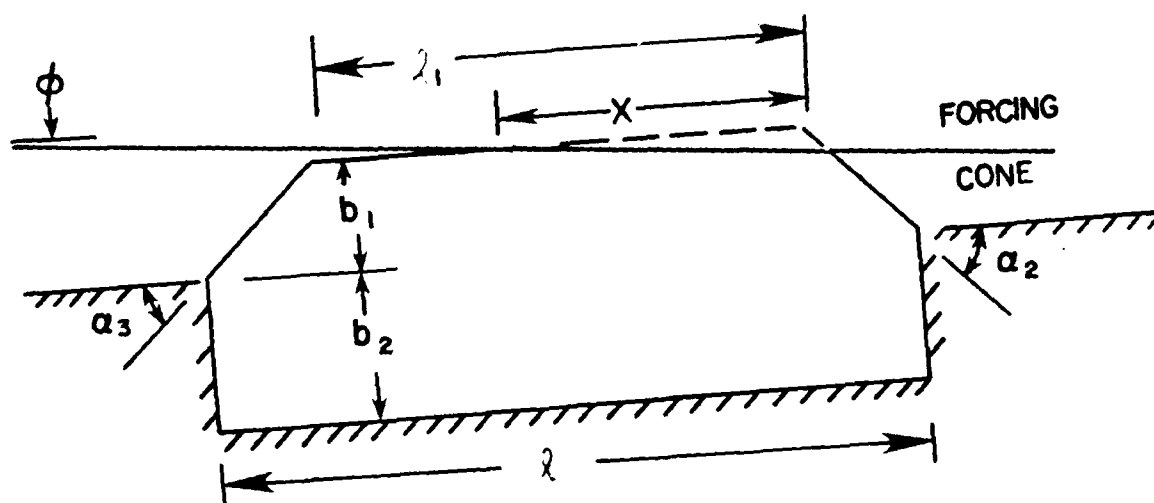
$$x_1 = \ell_1$$

and applying the law of sines to the small triangle with side s_2 ,

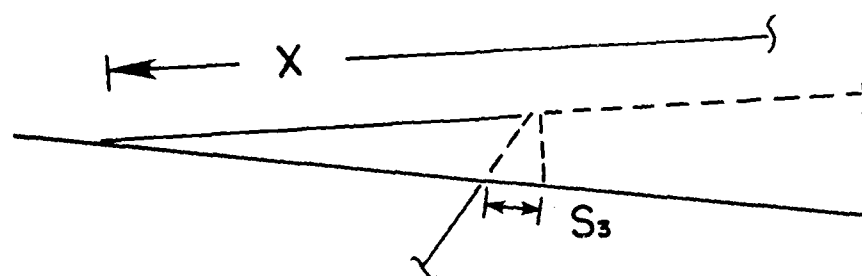
$$\begin{aligned} s_2 &= xm^-/\cos\phi \\ m^- &= \cos\alpha_2 \sin\phi/\sin(\alpha_2 - \phi) \end{aligned} \quad (14)$$

Thus,

$$F_x = \frac{\sigma_f \pi d_b}{\cos\phi} (1 + m^-)(\alpha_n \cos\phi + \sin\phi)x \quad 0 \leq x \leq x_1 \quad (15)$$



(a) INTERMEDIATE CUT



(b) BACK CUT

Fig. 4 Band contact geometry

3.2 Regime II

After the rifling has cut through the band top surface, it will continue to add contact length, but at a much lower rate, as the back bevel is cut along with the front bevel. The process will continue until the band reaches the end of the forcing cone region x_2 . This displacement does not coincide with L since the band reaches this point sooner by an amount $x_2 m^-$. Applying the law of sines to the small triangle including s_3 ,

$$A = \pi d_b \left[\frac{\ell_1}{\cos \phi} + s_2 + s_3 \right] \quad (16)$$

where

$$\begin{aligned} s_3 &= (x - \ell_1) m^+ / \cos \phi \\ m^+ &= \cos \alpha_3 \sin \phi / \sin(\alpha_3 + \phi) \end{aligned} \quad (17)$$

Thus,

$$F_x = \frac{\sigma_f \pi d_b}{\cos \phi} [\ell_1 + x m^- + (x - \ell_1) m^+] [\mu_n \cos \phi + \sin \phi] \quad (18)$$

$$x_1 \leq x \leq x_2$$

where

$$x_2 = \frac{L}{1 + m^-} \quad (19)$$

and L is given by equation (1).

3.3 Regime III

As the band proceeds into the straight bore, only the back bevel continues to add contact area. The band is assumed to flow around the shallow corner marking the forcing cone boundary and maintain full contact with the straight bore. Then

$$A = \pi d_b \left[\frac{\ell_1}{\cos \phi} + \frac{x_2 m^-}{\cos \phi} + s_3 \right] \quad x_2 \leq x \leq x_3 \quad (20)$$

Starting with x_2 the band must traverse the front bevel, the original surface length, and the back bevel before leaving the forcing cone,

$$x_3 = x_2 + x_2 m^- + \ell_1 + (x_3 - \ell_1) m^+$$

or

$$x_3 = \frac{L + \ell_1 (1 - m^+)}{1 - m^+} \quad (21)$$

At the same time the contact surface changes slope from ϕ to zero as the band passes into the straight bore. Now the force must decay linearly from

$$F_x = F_2 = \sigma_f A_2 (u_n \cos \phi + \sin \phi)$$

where force and area are evaluated at x_2 , to

$$F_x = F_3 = \sigma_f A_3 u_n$$

where the force and area are evaluated at x_3 . Thus,

$$F_x = F_2 + \frac{(F_3 - F_2)}{(x_3 - x_2)} (x - x_2) \quad x_2 \leq x \leq x_3 \quad (22)$$

All ϕ terms occurring implicitly in the contact area development, equation (20), are not affected.

3.4 Regime IV

When the band is completely through the engraving section, the area becomes constant.

$$F_x = \sigma_f \pi d_b \mu_n (x_3 - x_2) / \cos \phi \quad x \geq x_3 \quad (23)$$

Once the basic geometry for contact area is determined, it remains to establish the quasi-static flow pressure and coefficient of friction.

3.5 Flow Pressure

To describe the effect of multi-axial stresses on the yield of polymers, workers have postulated several criteria or stress combinations that must be reached before yielding occurs [10]. Experimental results of Raghava [11] have shown that the flow stress of several glassy polymers is in agreement with the von Mises yield criterion. Writing a more general form of the criterion which includes shear stresses [12],

$$(\sigma_1 - \sigma_2)^2 + (\sigma_2 - \sigma_3)^2 + (\sigma_3 - \sigma_1)^2 = 6[k^2 - (\tau_{12}^2 + \tau_{23}^2 + \tau_{31}^2)] \quad (24)$$

where k is the von Mises constant usually obtained from uniaxial tests. However, it is known that for many polymers the mechanical properties increase under a hydrostatic pressure [13-16]. Bowden and Jukes [15] conducted tests to determine a satisfactory yield criterion for polymers under compressive loads. They proposed a modified von Mises criterion in which k increases linearly with pressure p :

$$k = k_0 + \zeta \bar{\sigma} \quad , \quad \bar{\sigma} = -\frac{1}{3} (\sigma_1 + \sigma_2 + \sigma_3) \quad (25)$$

where $0.09 < \zeta < 0.25$ for several glassy polymers [15]. Then for uniaxial compression in the σ_1 direction ($\sigma_2 = \sigma_3 = 0$) until failure, $\sigma_1 = \sigma_s$ where σ_s is the compressive yield stress, equations (24) and (25) give

$$k_0 = -\frac{\sigma_s}{\sqrt{3}} (1 - \zeta/\sqrt{3}) \quad (26)$$

Although the rotating band engraving process has been compared to the extrusion process, it differs in several respects. Extrusion causes material failure throughout its bulk while the engraving involves a surface shear flow with the bulk material sliding past the failed material. Retrieved projectiles have been found with a doubled over ribbon of band material still attached to a non-groove section of the band. The material was smeared to the rear in a continuous failure. The stresses at the surface are normal to the cone surface $\sigma_1 = -\sigma_f$ and tangent to the cone circumference $\sigma_2 = -\sigma_f$. A shear stress in the direction of motion is $\tau_{13} = \mu\sigma_f$. For an axisymmetrical problem [12] with complete plasticity ($\sigma_1 = \sigma_2$), the above conditions reduce to

$$\sigma_f^2 = 3k^2 - 3\tau_{13}^2 \quad (27)$$

where $k = k_0 + \frac{\zeta}{3} (2\sigma_f)$. Thus,

$$\sigma_f = \frac{\sigma_s (1 - \zeta/\sqrt{3})}{\sqrt{1 + 3\mu^2 - 2\zeta/\sqrt{3}}} \quad (28)$$

3.6 Friction Coefficient

In the conventional presentation of the adhesion theory of friction, it is assumed that the real contact area increases with load in a way that the average contact stress remains constant and equal to the flow strength of the softer material. Thus, the friction coefficient is constant and independent of load as required by Amontons' law. Early studies of polymer friction [17-19] showed that these materials don't obey Amontons' law, i.e., $\mu \sim W^{-n}$ where $n < 1$. A number of different workers [20-23], taking the lead of Adams [18], verified that the shear strength of polymers increased with hydrostatic pressure. Towle [23] [24] proposed a simple extension of adhesion theory. If the shear strength

$$\tau_s = \tau_o + \gamma \bar{\sigma}$$

it follows that

$$\mu = \frac{\tau_o}{\bar{\sigma}} + \gamma \quad (30)$$

The equation predicts that the friction coefficient decreases with increasing load (pressure), approaching an asymptotic value at high loads. Several observed values for γ are: chromuim tris (phosphinate) [24] $\gamma = 0.07$; polymethylmethacrylate [16] $\gamma = 0.16$; nylon [25] $\gamma = 0.12$; unfilled and 30% glass filled polyacetal [26] $\gamma = 0.10$. All of the above references used low sliding speeds.

4.0 DYNAMIC ENGRAVING THEORY

The fundamental difference between quasi-static and dynamic conditions is the velocity sensitivity of the material mechanical properties and the coefficient of friction. Thus, their static values must be replaced by their dynamic counterparts σ_f' and μ_n' respectively.

4.1 Dynamic Flow Pressure

It is well known that the mechanical properties of materials are influenced by the rate of strain. When a material suffers impact, initial strains depend on the strain propagation velocity; large strains propagate at lower velocities than small strains. An impact velocity exists above which the large plastic strains being generated can not propagate as rapidly as the material is loaded. Johnson [27] notes that the ratio of dynamic to static flow stress for the strain-rate effects below the recrystallization temperature are $1 \leq \sigma_f'/\sigma_f \leq 2$. The ratio can only be determined by experiment.

Interest in dynamic testing at large strain rates $10^3 - 10^4 \text{ s}^{-1}$, which are comparable to the engraving process, began with the development of the split Hopkinson bar [28]. Maiden and Green [29] found that aluminum and pyrolytic graphite were insensitive to compressive strain rates up to 10^3 s^{-1} while lucite and micarta improved in strength by 100% and 50% respectively. Limited testing of materials for high strain rate effects has appeared in the literature; much of the existing work has been done with aluminum as reported by Nicholas [30]. Tensile strength increases are approximately 20% for aluminum as well as for stainless steels. Dynamic mechanical properties of polymers are

difficult to find. Yee [31] reported on the tensile strength change in two glassy polymers up to strain rates of 10^2 s^{-1} : both poly (2,6 - dimethyl phenylene oxide) and polystyrene increased by 25%.

4.2 Dynamic Friction Coefficient

For low sliding velocities the coefficient of friction increases with speed, caused by the increased contact area of asperities. At some critical velocity, on the order of several feet per second for polymers, the friction coefficient peaks and begins to decay with increasing speed [26][32-36]. Evidence is overwhelming that material melting occurs at the contacting asperities for these relatively low sliding velocities. Melting increases with sliding speed until the entire apparent contact area is a layer of melted material. The speed at which the full melt layer exists is not established, but it does depend on the load.

The most comprehensive experimental study of friction at high sliding speeds was done at the Franklin Institute from 1946 to 1956 by Clark, Morsell, and Shugarts. There was no publication of this work in the open literature because it was classified during that time. Montgomery [37] has recently collected all of this data. A pin-disk machine was used to slide various metal specimens against a steel disk. The coefficient of friction decreased with increasing values of pressure x velocity for all tested metals. A typical low coefficient of friction was approximately 0.2. One reported run with a nylon pin gave $\mu = 0.10$ at 900 ft/sec and 4100 psi. Montgomery found that the pin wear rate correlated directly with the reciprocal of the material absolute melting point.

Montgomery [38][39] also reported on experimental work to determine the friction coefficient of projectile rotating bands made from gilding metal (90 CU; 10 ZN). Measurements of gas propellant pressure, projectile acceleration, and the band normal contact pressure on rounds fired in a 155 mm howitzer were used to calculate the friction coefficient. The results were compared with similar data from the pin-disk experiments of the Franklin Institute. The friction coefficient for rotating bands drops quickly to a steady-state value of 0.02 at a pressure x velocity of approximately 4.0×10^6 (psi)(fps). For measured contact stresses of 50,000 psi during engraving, this limit gives a sliding velocity of 80 ft/sec. Polymers have much lower thermal conductivities and melting points than metals and the corresponding limit should be smaller. Montgomery attributed the lower coefficient of friction for rotating bands to the size effect inherent in a hydrodynamic sliding model of melt as proposed by Wilson [40]. It is significant that earlier high speed friction work by Bowden and Persson [41] found coefficient of friction values substantially less than 0.1 for various metals and non-metals.

5.0 RADIAL DISPLACEMENTS

There are a number of forces which come into play in interior ballistics. The effect of these forces is to produce radial displacements at the band which can drastically change the engraving and post-engraving sliding resistance. In addition, these forces vary between laboratory tests and actual firings in the field. Another factor is the projectile type. TP (target practice) projectiles are commonly employed in the laboratory and have a solid base under the band, Figure 1. However, field projectiles have a hollow base with a thin wall under the band and are referred to as HEI (high explosive incendiary) projectiles. The following displacements at the band are obtained from shell [42] or elasticity [43] theory.

5.1 Band Compression

The exposed portion of the band is in a state of plane stress while the submerged portion is in a state of plane strain:

$$\delta_b = \frac{\sigma_b}{E_b} (1 - \nu_b) \frac{b_1}{2} + \frac{\sigma_b}{E_b} (1 - 2\nu_b) \frac{(1 + \nu_b)}{(1 - \nu_b)} b_2 \quad (31)$$

where the average stress

$$\sigma_b = \sigma_f A \cos\phi / \pi d_b \ell = \sigma_f s \cos\phi / \ell$$

and $b_1/2$ is an average exposed length.

5.2 Projectile Compression

The projectile compression for a solid projectile is simply

$$\delta_p = \frac{\sigma_b d_p}{E_p} \frac{1}{2} (1 - \nu_p) \quad (\text{TP projectile}) \quad (32)$$

while band contact on a cylindrical shell causes a displacement

$$\begin{aligned} \delta_p &= \frac{\sigma_b d_p^2}{4E_p h} [1 - e^{-\beta \ell/2} \cos(\beta \ell/2)] \\ &\approx \frac{\sigma_b d_p^2 \beta \ell}{8E_p h} \quad (\text{HEI projectile}) \end{aligned} \quad (33)$$

where

$$\beta^4 = 12(1 - \nu_p^2)/d_p^2 h^2.$$

5.3 Barrel Compression

The action of the band against the barrel causes a counter shell (barrel) displacement

$$\begin{aligned} \delta_o &= \frac{\sigma_f d_2^2}{2E_o (d_2 - d_1)} [1 - e^{-\beta s/2} \cos(\beta s/2)] \\ &\approx \frac{\sigma_f d_2^2 \beta s}{4E_o (d_2 - d_1)} \end{aligned} \quad (34)$$

where

$$\beta^4 = 48(1 - \nu_o^2)/d_2^2 (d_2 - d_1)^2$$

5.4 Barrel Gas Pressure

A uniform gas pressure P acting on the barrel interior behind the band will cause an additional displacement of the barrel at the band.

Since the displacement before band contact is made only affects X_1 ,

$$\delta_g = \frac{(P - P_1)d_1}{2E_o} \left[\frac{d_2^2 + d_1^2}{d_2^2 - d_1^2} - \nu_o \right] \quad (35)$$

where P_1 is the pressure at the start of the engraving process. Now the gas pressure during engraving increases in a quasi-linear fashion until it peaks well after the engraving process. So

$$P - P_1 = \frac{P_2 - P_1}{x_2} x \quad 0 \leq x \leq x_2 \quad (36)$$

where P_2 is the gas pressure at $x = x_2$.

5.5 Projectile Acceleration

The gas pressure acting on the base of the projectile will cause a lateral strain in the projectile and band at a cross-section through the projectile at the band location. In most cases equation (10) is approximately represented by

$$M\ddot{x} = PA_p \quad (37)$$

Then the internal stress P' at the cross-section with area A_p' leads to the following force balance:

$$P'A_p' = M'\ddot{x} \quad (38)$$

where M' is the projectile mass ahead of the cross-section. Thus,

$$P' = P \frac{A_p M'}{A_p' M} \quad (39)$$

The lateral strain, measured from the start of the engraving process, is

$$\delta_a = \left(\frac{d}{2} \frac{\nu_p}{E_p} + \frac{b_2 \nu_b}{E_b} \right) \left(\frac{A_p M'}{A_p' M} \right) (P - P_1) \quad (\text{TP projectile}) \quad (40)$$

$$\delta_a = \left(h \frac{\nu_p}{E_p} + b_2 \frac{\nu_b}{E_b} \right) \left(\frac{A_p M'}{A_p M} \right) (P - P_1) \quad (\text{HEI projectile}) \quad (41)$$

5.6 Projectile Spin

The displacement at the outer radius r_o of a hollow disk is given by

$$\delta_s = \frac{\rho \omega^2 r_o^2}{4E_p} [r_i^2 (3 + \nu_p) + r_o^2 (1 - \nu_p)] \quad (42)$$

This equation is an approximation to the actual projectile deflection, but substitution of typical parameters shows that its contribution is negligible.

6.0 REVISED THEORY

6.1 Engraving Theory

At this point the engraving theory has been derived on the premise that radial displacements of projectile and barrel are non-existent. Corrections for radial displacements will be undertaken now. Once the engraving process begins, the combined effect of the radial forces will allow material elastic movement by an amount

$$\delta = \delta_b + \delta_p + \delta_o + \delta_g - \delta_a \quad (43)$$

Thus, instead of contact length s for rigid surfaces after a projectile displacement x we have a smaller contact length \tilde{s} . By similar triangles

$$(\Delta\tilde{x})\tan\phi = (\Delta x)\tan\phi - \Delta\tilde{\delta} \quad (44)$$

where the "over bar" denotes quantities associated with \tilde{s} . The derived radial displacement can be written as

$$\Delta\tilde{\delta} = \kappa_1 \Delta\tilde{s} + \kappa_2 \Delta\tilde{x}$$

From the expressions for contact lengths s_1, s_2, s_3

$$\Delta\tilde{s}_n = \frac{ds_n}{dx} \Delta\tilde{x}$$

which shows that each regime must be considered separately. Substituting the above two expressions into equation (44),

$$\Delta\tilde{x} = (\Delta x)/c_n \quad (45)$$

where

$$c_n = 1 + \frac{\kappa_1}{\tan\phi} \left(\frac{ds_n}{dx} \right) + \frac{\kappa_2}{\tan\phi}$$

The effect of the radial displacement is to produce a smaller slope in each regime. Denoting only the end points of each linear regime,

$$F_1 = B[(1 + m^-)x_1/c_1] \quad \text{at } x_1 \quad (46)$$

$$F_2 = F_1 + B[(m^- + m^+)(x_2 - x_1/c_2)] \quad \text{at } x_2 \quad (47)$$

$$F_3 = \sigma_f \mu_n A_3 \quad \text{at } x_3 \quad (48)$$

where

$$B = \sigma_f \pi d_b (\mu_n + \tan\phi) \quad (49)$$

$$A_3 = \pi d_b (x_3 - x_2)/\cos\phi \quad (50)$$

$$x_1 = \ell_1 c_1 \quad (51)$$

$$x_2 = L - (x_1 m^-/c_1) - (x_2 - x_1) m^-/c_2$$

or

$$x_2 = \frac{L - m^- x_1 [(1/c_1) - (1/c_2)]}{1 - (m^-/c_2)} \quad (52)$$

$$x_3 = x_2 + \frac{x_1 m^-}{c_1} + \frac{(x_2 - x_1) m^-}{c_2} + \ell_1 + \frac{(x_2 - \ell_1) m^+}{c_2} + \frac{(x_3 - x_2) m^+}{c_3}$$

or

$$x_3 = \frac{L + \ell_1 (1 - \frac{m^+}{c_2}) + x_2 m^+ (\frac{1}{c_2} - \frac{1}{c_3})}{1 + (m^+/c_3)} \quad (53)$$

6.2 Post-Engraving Theory

The band is engraved with $A = A_3$ at x_3 . However, the gas pressure at the projectile base continues to radially displace the projectile and barrel. Let δ' be the residual elastic strain in the band, barrel, and projectile:

$$\delta' = \delta_b + \delta_p + \delta_o \Big|_{A=A_3} \quad (54)$$

This strain will be relieved by the developing gas pressure and band wear δ_w , and it will be increased down bore by the projectile displacement from the spin forces:

$$\delta'' = (\delta_g + \delta_w) \Big|_{P=P-P_2} - \delta_a - \delta_s \quad (55)$$

Generally δ_s is negligible, and δ_w is unknown but thought to be negligible. The contact stress σ between the band and barrel takes up the remaining elastic strain δ''' or

$$\delta''' = \delta_b + \delta_p + \delta_o \Big|_{\substack{A=A_3 \\ \sigma_f = \sigma}} \quad (56)$$

Then the contact stress σ can be found from

$$\delta' - \delta'' = \delta''' \quad (57)$$

Finally the post-engraving sliding force is

$$F_x = \sigma A_3 \mu_n \quad (58)$$

7.0 APPLIED THEORY

A recent report by Cross [44] offers an opportunity to verify the engraving theory. Although the laboratory experiments were conducted to determine important rifling parameters, both the quasi-static and dynamic engraving results for the 20 mm projectiles (TP) were given. The rotating bands were plastic (20% glass-filled polyethersulfone). The rifling was a standard 9-groove square cross-section.

The quasi-static engraving process used a standard MTS Systems testing machine in which the projectiles could be forced into the rifled barrel section and the measurement of force versus displacement made. The engagement speed was at 63.5 mm/sec.

For the dynamic tests a forcing cone section was propelled down a pipe at 50 m/sec where it struck a stationary projectile. The projectile nose had been threaded onto a Hopkinson tube which absorbed the impact force on the rotating band. The force versus time was recorded by means of strain gages, and the force-displacement curve was calculated from the constant velocity.

Pertinent parameters [44] and band properties [45][46] are given below:

$$\begin{array}{ll}
 d_b = 21 \text{ mm} & \phi = 2.5^\circ \\
 d_p = d_o = 20 \text{ mm} & \alpha_2 = \alpha_3 = 20^\circ \\
 d_1 = 20.5 \text{ mm} & \tau = 0.15 \\
 d_2 = 57 \text{ mm} & +\gamma_s = -\gamma_s = 1.38 \times 10^8 \text{ N/m}^2 \\
 \ell = 7.2 \text{ mm} & E_b = 6.89 \times 10^9 \text{ N/m}^2
 \end{array}$$

$$\begin{aligned}
 \ell_1 &= 4.5 \text{ mm} & E_p &= E_o = 2.07 \times 10^{11} \text{ N/m}^2 \\
 b_1 &= 0.46 \text{ mm} & \nu_b &= 0.4 \\
 b_2 &= 0.97 \text{ mm} & \nu_p &= \nu_o = 0.3
 \end{aligned}$$

7.1 Static Results

The static test results from Cross [44] are shown in Figure 5. The basis for the theory is as follows.

- (1) There is no data available on the friction coefficient for the above polymer, but the literature suggested a value between $\mu = 0.1$ and $\mu = 0.15$ for similar polymers under extreme pressure. The flow pressure is found from equation (28) using a trial value of $\mu = 0.14$: $\sigma_f = 1.47 \times 10^8 \text{ N/m}^2$.
- (2) Using point (1) at the end of regime I from Figure 5 and equation (46) from theory, the actual friction coefficient is $\mu = 0.14$. With flow pressure and friction coefficient defined, the remaining theory follows Section 6.0.
- (3) Radial displacements are dominated by the barrel gas pressure, and

$$e_n = \nu_p \sigma_f \gamma_2 \tan \alpha$$

where γ_2 is calculated to be 2.57×10^{-3} . Thus, the end of regime I is $\gamma_1 e = 4.80 \text{ mm}$. This point is confirmed by the experiment.

There are several observations to be made. First, the oscillatory character of regime II is caused by the continuous formation of new edge being cut on the back bevel. Second, the test data is smooth

at points (2) and (3) since the sharp corner at the end of the forcing cone is usually removed. Third, the stressed band material slowly relieves itself as the band enters the straight bore. This effect causes a slightly greater slope in regime III and a fading resistance force in regime IV once the band has been engraved. The phenomenon should not be present during dynamic tests or actual firings.

7.2 Dynamic Results

The dynamic test results from Cross [44] are shown in Figure 5. The basis for the theory is as follows:

- (1) The line of force on the Hopkinson tube at the smaller diameter projectile nose was inside the line of opposing force on the projectile rotating band. The net effect is a strong bending moment on the projectile base at the band which produced an additional deflection under the rotating band. This deflection is difficult to calculate but the data for $x_1 = 6.35$ mm indicates that $c = 1.43$, equation (51). This value is confirmed by the added delay for $x_2 = 10.67$ mm, equation (52), shown for the data in Figure 5.
- (2) The literature review suggested that polymers begin to melt at sliding speeds of approximately 15 m/sec for light loads. For the constant pressure and speed here, full melt lubrication should be attained with a friction coefficient $\mu' \ll 0.1$. Using the immediate post-engraving steady-state force $F_x' = 955$ N and equation (58) where $\mu' = \mu_f$ (the material is no longer under impact),

$$\mu_n' = 0.016.$$

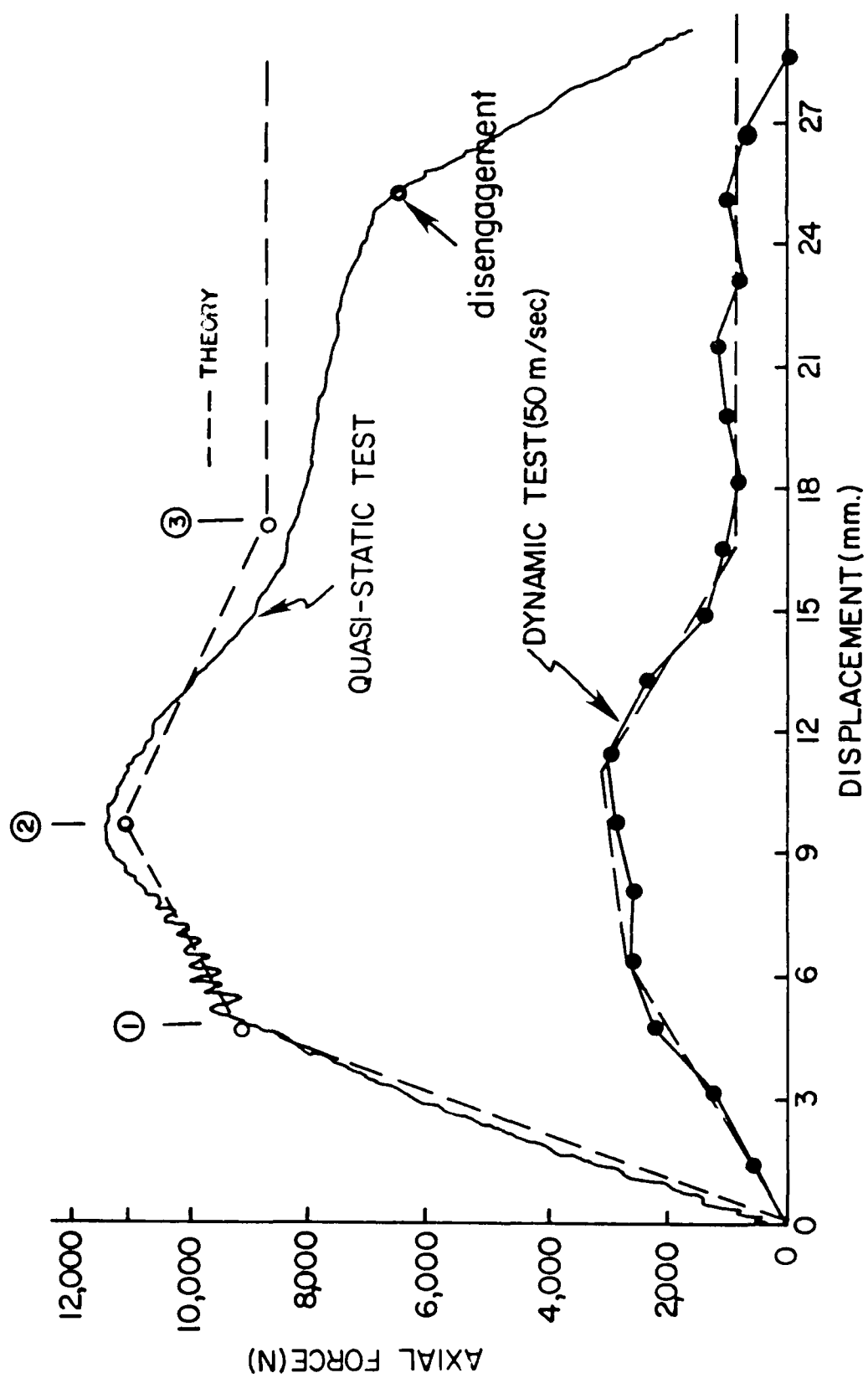


Fig. 5 Comparison of theory with experiment

- (3) Using point (1) at the end of regime I and equation (46), the dynamic flow pressure for the engraving process is $\sigma_f' = 1.40 \times 10^8 \text{ N/m}^2$. Comparing uniaxial yield stress by means of equation (28): $\sigma_s'/\sigma_s = 1.14$. This value agrees with values reported in Section 4.0 for other polymers.

8.0 CONCLUSIONS

A theory has been presented for the first time which quantifies the projectile sliding force as a function of displacement in interior ballistics. The theory illustrates the need to consider geometrical details of the projectile rotating band and barrel forcing cone and serves to isolate the dynamic flow pressure and the coefficient of friction as the main parameters.

Confirmation of the theory is impeded by a lack of data on these parameters under ballistic conditions and by a lack of projectile sliding force tests in the literature which includes the necessary geometrical details. The recent work by Cross [44], using polyether-sulfone rotating bands, afforded the opportunity to compare the theory with experiment. A single point on the static test was used to obtain the static coefficient of friction. Two points on the dynamic test were used to obtain the dynamic coefficient of friction and the polymer dynamic flow pressure. The resulting three parameters were comparable to values reported in the literature for similar polymers and test conditions. Confidence in the theory was enhanced by its ability to predict the various force-displacement segments and to predict the location of each regime which depends on the parameters as well as the geometry. Although independent studies on material dynamic failure and friction would be preferred, it is believed that the theory could provide the researcher with the means to obtain these parameters

indirectly from laboratory or ballistic tests of actual projectiles as illustrated above.

Finally, the occurrence of radial displacements between the projectile and barrel can have a significant effect on the projectile sliding forces. Thus, care must be exercised to distinguish among laboratory quasi-static tests, laboratory dynamic tests, and actual field tests.

9.0 ACKNOWLEDGMENTS

This research was sponsored by the Air Force Office of Scientific Research/AFSC, United States Air Force, under contract F49620-79-C-0038 and Grant AFOSR-82-0169. The United States Government is authorized to reproduce and distribute reprints for governmental purposes notwithstanding any copyright notation hereon.

In addition, the author would like to thank Otto K. Heiney, Interior Ballistic Branch, Air Force Armament Laboratory, Eglin AFB, for topic suggestion and useful comments while the author was participating in the 1981 Summer Faculty Research Program administered by the Southeastern Center for Electrical Engineering Education.

10.0 REFERENCES

1. H. Krier and M. J. Adams, An Introduction to Gun Interior Ballistics and A Simplified Ballistics Code. Prog. in Astro. and Aero. 66 (1979).
2. E. B. Fisher, Ibid.
3. D. Perrin and S. Duke, Barrel Life in High Rate of Fire Gatling Guns. Proc. of the Tri-Service Gun Tube Wear and Erosion Sym. U. S. Army Arm. Res. and Dev. Com., Dover, NJ (1977).
4. D. M. Davis, Review of the Air Force Program in Gun Barrel Life. Ibid.
5. O. K. Heiney, Ballistics Applied to Rapid-Fire Guns. Prog. in Astro. and Aero. 66 (1979).
6. P. G. Baer, Practical Interior Ballistic Analysis of Guns. Ibid.
7. E. B. Fisher and A. P. Trippe, Mathematical Model of Center Core Ignition in the 175 mm Gun. Calspan Rept. VQ-5163-D-2 (1974).
8. O. K. Heiney et al., Experimental Interior Ballistic Variability Phenomena in the 30 mm GAU-8 Gun. AFATL-TR-79-64 (1979).
9. W. F. Hartman and P. P. Stirbis, Rotating Band Pressures and Engraving Forces in 155 mm Artillery Shells. J. of Eng. Mat. and Tech. 95, 124 (1973).
10. I. M. Ward, Mechanical Properties of Solid Polymers. Wiley-Interscience, London (1971).
11. R. Raghava et al., The Macroscopic Yield Behavior of Polymers. J. Mater. Sci. 8, 225 (1973).
12. E. P. Unksov, An Engineering Theory of Plasticity, p. 93. Butterworths, London (1961).
13. J. A. Sauer, Deformation, Yield and Fracture of Polymers at High Pressure. Poly. Eng. and Sci. 17, 150 (1977).
14. S. Rabinowicz et al., The Effect of Hydrostatic Pressure on the Shear Yield Behavior of Polymers. J. Mater. Sci. 5, 29 (1970).
15. P. B. Bowden and J. A. Jukes, The Plastic Flow of Isotropic Polymers. J. Mater. Sci. 7, 52 (1972).
16. B. J. Briscoe and D. Tabor, The Effect of Pressure on the Fractional Properties of Polymers. Wear 34, 29 (1975).

17. M. W. Pascoe and D. Tabor, The Friction and Deformation of Polymers. Proc. Roy. Soc. (London) A235, 210 (1956).
18. N. Adams, Friction and Deformation of Nylon I. Experimental. J. Appl. Poly. Sci. 7, 2075 (1963).
19. N. Adams, Friction and Deformation of Nylon II. Theoretical. J. Appl. Poly. Sci. 7, 2105 (1963).
20. S. Rabinowicz et al., The Effect of Hydrostatic Pressure on the Shear Yield Behavior of Polymers. J. Mat. Sci. 5, 29 (1970).
21. D. R. Mears et al., Effects of Hydrostatic Pressure on the Mechanical Behavior of Polyethylene and Polypropylene. J. Appl. Phys. 40, 4229 (1969).
22. J. Sauer, Deformation, Yield and Fracture of Polymers at High Pressure. Poly. Eng. Sci. 17, 150 (1977).
23. L. C. Towle, Shear Strength and Friction Measurements on Thin Layers Under High Pressure. J. Appl. Phys. 42, 2368 (1971).
24. L. C. Towle, Friction and Shear Strength of a Chromium Tris (Phosphinate) Polymer Under High Pressure. ASLE Trans. 17, 224 (1974).
25. P. J. Aird and B. W. Cherry, Frictional Properties of Branched Polyethylene II. The Normal Force/Shear Force Relationship. Wear 51, 147 (1978).
26. M. Clerico, Tribological Behavior of Polyacetals. Wear 64, 259 (1980).
27. W. Johnson, Impact Strength of Materials. London, Edward Arnold (1972).
28. H. Kolsky, An Investigation of the Mechanical Properties of Materials at Very High Rates of Loading. Proc. Phys. Soc. (London) 42, 676 (1949).
29. C. J. Maiden and S. J. Green, Compressive Strain Rate Tests on Six Selected Materials at Strain Rates from 10^{-3} to 10^4 s⁻¹. J. Appl. Mech. 33, 496 (1966).
30. T. Nicholas, Tensile Testing of Materials at High Strain Rates. Exp. Mech. 21, 177 (1981).
31. A. F. Yee, Mechanical Properties of Mixtures of Two Compatible Polymers. Poly. Eng. and Sci. 17, 213 (1977).
32. G. V. Venogradov et al., A Study of Heavy Metal-to-Plastic Friction Duties and of the Wear of Hardened Steel in the Presence of Polymers. Wear 8, 358 (1965).

33. K. G. McLaren and D. Tabor, Friction of Polymers at Engineering Speeds: Influence of Speed, Temperature and Lubricatns. Wear 8, 79 (1965).
34. M. Clerico, A Study of the Friction and Wear of Nylon Against Metal. Wear 13, 183 (1969).
35. K. Tanaka and Y. Uchiyama, Friction, Wear and Surface Melting of Crystalline Polymers. Advances in Polymer Friction and Wear (ed., L. H. Lee). Plenum, New York (1974).
36. K. Tanaka, Friction and Wear of Glass and Carbon Fiber-Filled Thermoplastic Polymers. J. Lub. Tech. 99, 408 (1977).
37. R. S. Montgomery, Friction and Wear at High Sliding Speeds. Wear 36, 275 (1976).
38. R. S. Montgomery, Surface Melting of Rotating Bands. Wear 38, 235 (1976).
39. R. S. Montgomery, Projectile Lubrication by Melting Rotating Bands. Wear 39, 181 (1976).
40. W. R. D. Wilson, Lubrication by a Melting Solid. J. Lub. Tech. 98, 22 (1976).
41. F. B. Bowden and P. A. Persson, Deformation, Heating and Melting of Solids in High Speed Friction. Proc. Roy. Soc. (London) A260, 433 (1961).
42. S. P. Timoshenko and Wornowski-Krieger, Theory of Plates and Shells 2nd ed. McGraw-Hill (1959).
43. S. P. Timoshenko and J. N. Goodier, Theory of Elasticity 3rd ed. McGraw-Hill (1970).
44. L. A. Cross, Optimum Gun Barrel Rifling Designs for High Performance Aircraft Gun Systems. AFATL-TR-80-83 (1980).
45. The International Plastics Selector. Cordura Publications (1977).
46. Modern Plastics Encyclopedia. McGraw-Hill (1978-79).

LIST OF FIGURES

- Figure 1. Barrel entrance with rifling start.
- Figure 2. Engraved projectile rotating band.
- Figure 3. Engraving geometry.
- Figure 4. Band contact geometry.
- Figure 5. Comparison of theory with experiment.

END

FILMED

4-83

DTIC